2016 IEEE/RSJ International Conference on Intelligent Robots and Systems (IROS)
Daejeon Convention Center
October 9-14, 2016, Daejeon, Korea

A Humanoid Doing an Artistic Work - Graffiti on the Wall

Youngbum Jun[1], Giho Jang[1], Baek-Kyu Cho[2], Joel Trubatch[1], Inhyeok Kim[3], Sang-Duck Seo[1] and Paul Y. Oh[1]

***Abstract*— Graffiti work using a humanoid with artistic technique can convey the value of artists' work to people. Previous work that focused on drawing an image on a canvas accurately has not contained artistic processes like performance, drawing skills and other artists' intents at the time of creation. To combine such artistic processes, the work in this paper utilizes whole-body motion of a humanoid to paint an image on a wall using Pointillism. However, a biped humanoid consists of high Degree Of Freedom (DOF) system and is very sensitive to internal and external disturbances from interaction with environments. As is the case when graffitiing on a wall. Most notably, the vibration from impact contacts and mechanical uncertainties limit the humanoid in graffitiing properly. This paper presents an approach to realize drawing a large image on a wall through real-time motion planning for printing, artificial compliance, and a disturbance controller.**

I. INTRODUCTION

Graphic wall art demands both creativity and the ability to effectively handle surfaces and apply paint. Robots still lack human-level creativity. However, mimicking drawing styles, manipulating art tools and paints, and compensating for surfaces like bumpy walls, is possible with robots. Programming a robot to paint wall art has applications. For instance, the art can be duplicated by the robot in different locations. There is also potential for human-robot or multi-robot collaborative painting. However, research on robotic art work has been mainly focused on copying an original image and the performance gaged by the accuracy of the replication.

Robot drawing has demonstrated an ability of robotic manipulators to create artistic work. Most of the work has focused on drawing a sketch through visual sensing using a simple-configured manipulator. The authors in [1] describe 2*D* portrait-sketching canvass and in [2] applied force control to compensate for disturbances to the canvass' location. The research in [3][4] designed a three fixed-axis machine to draw an image on on spherical surfaces like a tennis ball. A humanoid platform was utilized for sketching an image on a flat canvas in [5][6]. In contrast to robots drawing a given image, [7] describes free sketches of people.

Most of the previous research shows the capabilities of robotic platforms to sophisticatedly replicate artistic work. Beyond the resulting drawing, art is also valued by its process. Examples include generation (like stroke style), strategy (material type) and the time involved. Of course, it is very difficult to quantify artistic value. To create such value, the work in this paper presents the creation of robotic graffiti on a wall using whole-body motion of an adult-sized humanoid called DRC-Hubo which was designed and used for disaster-response in the DARPA Robotics Challenge (DRC) [8][9][10][11] with a painting technique derived from Pointillism.

A humanoid probably has the most reasonable form-factor to mimic human behavior. Unlike the aforementioned robots, DRC-Hubo was not designed to be a painter. In terms of realization of graffiti on a wall with an artistic technique, it is required to imitate the techniques in motions, proper handling of an artistic tool, and adapt to a human-centered

(a)

(b)

Fig. 1. (a) Final output of pointillism art, (b) DRC-Hubo art performance in Life Is Beautiful, September 24-27th 2015.

[1]Y. Jun (1075jun@gmail.com), G. Jang (gi.jang@unlv.edu), J. Trubatch (trubatch@unlv.nevada.edu), and P.Y. Oh (paul.oh@unlv.edu) are in Mechanical Engineering and SD. Seo (sang-duck.seo@unlv.edu) is in Department of Art, University of Nevada Las Vegas (UNLV), Las Vegas, NV 89154, USA. [2]BK Cho (baekkyucho@kookmin.ac.kr) is in Mechanical Systems Engineering, Kookmin University, South Korea. [3]I. Kim (inhyeok99@gmail.com) is in Naver Corp. South Korea.

environment. Most of this paper describes the technical aspects how to realize reliable and stable Pointillism artwork with a humanoid.

DRC-Hubo has done graffitiing a 1 m×15 m image on a old motel wall. This was for *Life is Beautiful* that brought over 100,000 people to Downtown Las Vegas. This celebrity-filled festival of art, music and food served as a platform; over the 3-day event, DRC-Hubo created a 10-foot Pointillist art mural. Painting 8+ hours daily in 100+ F heat demonstrated evolution (i.e. time-value) of art and hence value. For 3-days, thousands of people watched DRC-Hubo's drawing performance and progress and interacted with it.

The rest of paper consists of five additional sections. In Section. II, a definition of Pointillist art and the image processing method for graffiti are explained. In Section. III the motion planning for the hands to create graffiti on an unknown surface is detailed. In Section. IV the controllers for disturbance rejection both from the robot and the environment are covered. In Section. V the experimental results are presented and the work is concluded in Section. VI.

II. ROBOT GRAFFITI WITH POINTILLISM ART

Van Gogh's 1887 *Self Portrait* is a famous example of Pointillism. This technique uses patterns of small distinct dots of color for the image. To realize Pointillism art with a humanoid, the first consideration is to determine the resolution for the image. It has to be high enough to represent the image's original form and meaning. It constrains the tool size and in this case, paint markers were utilized. A smaller marker allows the robot to print more dots (higher resolution) in a defined area. Second, the size of the image to be drawn needs to be specified in terms of the manipulation work space. This determines a drawing motion sequence. Then the surface roughness, ground topology, and speed of motion to print a dot must be considered. These form the concept for the controller design.

A. Image Processing for Graffiti with Pointillist Technique under Robot Constraints

The size of the tool (a variable) used to make a mark while painting correlates to the minimum and maximum size of a point that can be made with that tool (refer to Section. V-A). A paint marker create points of uniform dimension when applied normal to a surface. DRC-Hubo matched markers to the required pixel size. The size of an image painted with this image processing technique is then defined as Eq.(1).

$$\begin{bmatrix} l_w \\ l_h \end{bmatrix} = \begin{bmatrix} (W_w + M_{dot})P_m \\ (W_h + M_{dot})P_n \end{bmatrix} \tag{1}$$

where l stands for a length of an actual drawing while subscripts h and w represent height and width, respectively. P_m and P_n denote a total number of pixels in a given image having m by n resolution. M_{dot} means the size of a dot specified by a marker and W is a weight value which is a distance between dots.

While the reachable points in the horizontal direction for manipulation are constrained. A humanoid can translate horizontally by walking to effectively remove this constraint. On the other hand, the reachable space in the vertical direction is fully limited. Therefore, the size of the original image has to be rescaled when l_h exceeds the vertical work space limit of the robot.

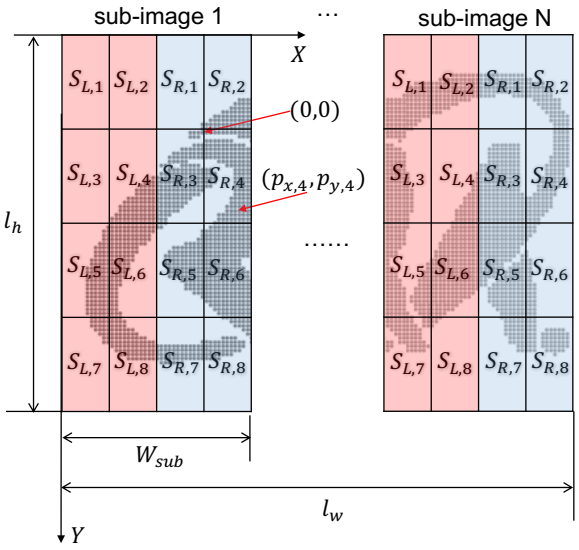

Fig. 2. The original image is rescaled based on the vertical work space limit and partitioned into sub-images in terms of the horizontal work space limit.

In a particular case where l_w exceeds the horizontal work space limit, the original image is partitioned into several sub-images illustrated in Fig. 2. A width for each sub-image, depicted as W_{sub}, can be arbitrarily determined as a value within the horizontal work space limit. Each divided image has an origin, $(0,0)$, at the top-left corner. The coordinates of pixels are based on that representation. Then, a humanoid starts to draw from the first to Nth sub-images, where N is the total number of sub-images, while walking horizontally.

Pointillism style art is created with a large number of discrete points. A two-handed motion has been utilized in order to maximize the rate at which the humanoid can create points. In order to reduce the potential for self-collision, each sub-image is divided again into sixteen sections and a sequence is assigned to each hand as shown in Fig. 2. The notation for each section is as follows: S is section, and the subscripts L, R, and numbers 1 through 8 are the left hand, right hand and sequence respectively.

As the coordinates of each point are now defined, the planar trajectories between each point can now be obtained. Eq.(2) is the transformation between the localized coordinate and the trajectory for the motion of a hand in a section.

$$\begin{bmatrix} C_{x,k} \\ C_{y,k} \\ C_{z,k} \end{bmatrix} = T_I^R \begin{bmatrix} (W_w + M_{dot}) & 0 \\ 0 & (W_h + M_{dot}) \end{bmatrix} \begin{bmatrix} P_{x,k} \\ P_{y,k} \end{bmatrix} \tag{2}$$

where $P_{x,k}$ and $P_{y,k}$ are a coordinate in the X- and Y-directions of kth section. The X and Y axes are defined

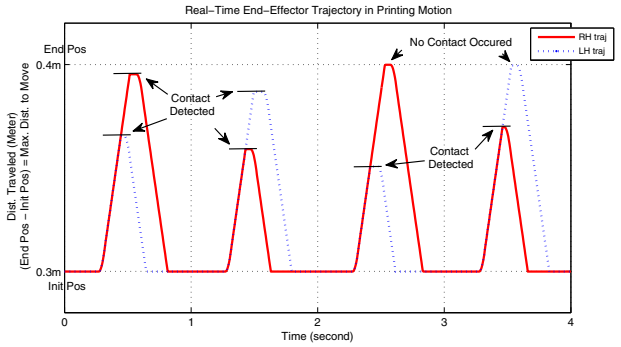

Fig. 3. Real-Time trajectories of right (red-solid-line) and left (blue-dotted-line) hands for printing. Each hand moves from *InitPos* to *EndPos* unless it detects a contact. Once a contact occurs, the hand stops moving and pulls back to *InitPos*.

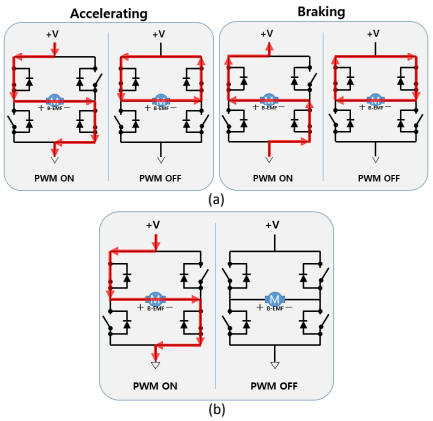

Fig. 4. Current flows in H-bridge in (a) Complementary Switching PWM (CSP) mode and (b) non-Complementary Switching PWM (nCSP) mode.

in Fig. 2. T_I^R represents a 3×2 transformation matrix that converts the coordinate system in the plane of the image to the local coordinate system of the robot. $C_{x,k}$, $C_{y,k}$ and $C_{z,k}$ are the position in the X-, Y- and Z- axes of the robot's local coordinate system.

Note that the trajectories generated during this process only move the hand in the plane parallel to the surface of the wall; only the $C_{x,k}$ and $C_{z,k}$ coordinates are utilized. The $C_{y,k}$ value is zeroed to allow for the marking motion in which a point is made on the wall. The motion in this axis is explained in Section. III.

III. MOTION PLANNING PRINTING DOTS ON UNEVEN VERTICAL WALL

Pre-processed image data provides the dots' local coordinates in the wall's X-(horizontal) and Z-(vertical) directions. In terms of drawing motion, a pre-defined trajectory cannot be applied because the surface condition of the wall might be rough and uneven. Thus, a real-time motion is generated with simple kinematics as following Eq.(3).

$$s_1 = s_0 + vt_s + \frac{1}{2}at_s^2 \qquad (3)$$
$$\text{update } s_0 = s_1,\ v = v + at_s$$

where s_1 and s_0 are the next and current displacements of the printing motion, respectively. a is the given acceleration, v is the velocity, and t_s is the sampling time (step time of the control loop).

The input value for the acceleration determines how quickly the hands will print a dot. However, to avoid joint saturation, the maximum hand velocity and travel distance have to be limited. Fig. 3 shows how it works. Red-solid-line and blue-dotted-line represent the trajectories of the right and left hands, respectively. *InitPos* is the current position and *EndPos* is a position the user specified based on robot's kinematic constraints. In Fig. 3, *InitPos* and *EndPos* are arbitrarily set to 0.3 m and 0.4 m, a is defined as $10\,\mathrm{m/s^2}$, and the velocity limit is specified as $0.4\,\mathrm{m/s}$. The control frequency is 200 hz. A wrist-joint force/torque (F/T) sensor detects contacts as the hand moves to *EndPos*. When detected, the hand stops immediately and returns to *InitPos*. This approach allows the robot to paint dots on uneven walls or surfaces.

IV. VIBRATION REDUCTION CONTROLS

A. Joint Compliance Control using Mechanical Methods

Vibration coming from uncertainties such as mechanical structural compliance, mathematical errors in dynamics, and interaction with the wall limits accurate and rapid drawing. The reduction of undesired vibration requires a force-absorption. People can account for vibrations because their physical makeup (bones, tissue, muscles) is inherently compliant. By contrast, robots often lack similar compliance. Torque-based control [12][13][14] for robotic compliance is well-known to handle such vibrations. However, an adult-sized motorized humanoid typically has a high-reduction ratio in each joint and thus, high-friction and low-backdrivability exist. It limits the performance of dexterous manipulation in the current state-of-art.

In this paper, the authors realize joint compliance with non-Complementary Switching PWM (nCSP) mode [15] which is equipped on the motor controller commercially available from Rainbow Inc. The nCSP is a H-bridge switching strategy that minimizes the braking effect resulting from the current (energy) generation in the motor operation. It increases the backdrivability of the joint. Fig. 4 demonstrates a comparison of the current flows in the H-bridge between the CSP and nCSP modes in terms of switching strategy.

To maximize joint compliance with nCSP, the friction coefficients to compensate for joint friction are empirically found and the motor control gains are manually tuned and proportional gain is adjusted. There is a trade-off between the error allowance (compliance) and joint precision (rigidity) in tuning the motor control gains. The compliance implementation through this mechanical approach does not compensate for gravitational force. Increasing joint compliance results in vertical sagging due to gravity. The capability to fully

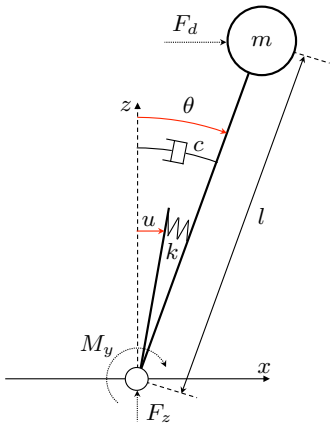

Fig. 5. A simplified linearized inverted pendulum with a disturbance.

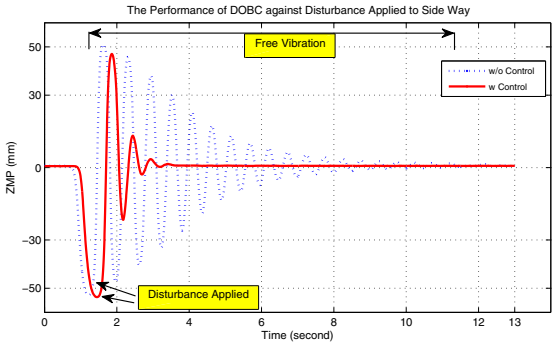

Fig. 6. Performance of the Disturbance observer ZMP controller in Y-(lateral) direction: blue-dotted and red-solid lines represent the ZMP profiles without the controller and with controller, respectively.

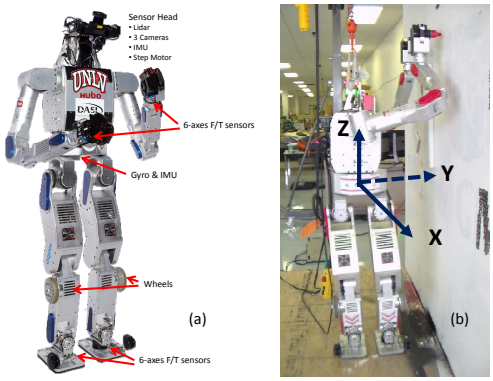

Fig. 7. (a) DRC-Hubo. (b) Initial pose for graffiti work with Pointillist technique

absorb disturbance is thus limited in order to minimize end-effector's position error.

B. Disturbance Observer ZMP Controller

The aforementioned compliance controller does not fully eliminate forces from impact and/or inertial whole-body motion. With a disturbance observer widely used for motion control [16][17], the authors designed a disturbance-observer Zero Moment Point (ZMP) controller to diminish the vibration from the remaining force. The type of the ZMP balance controller for humanoids can be simply classified into two control objectives; one is for force compliance and the other is for tracking the desired ZMP value. The disturbance observer-based ZMP controller designed in this paper has both compliance and integral action.

The Linearized Inverted Pendulum Model (LIPM) is a simplified dynamic model popular in humanoid community to control the stability. The mechanical and structural compliance can be represented as a spring-damper system. The modified LIPM with the spring-damper system is shown in Fig. 5 [18][19]. Eq.(4) represents the equation of motion of the modified LIPM with the disturbance acting on the system in the horizontal direction. The disturbance is modeled and added to LIPM.

$$ml^2\ddot{\theta} + c\dot{\theta} + k\theta - mgl\sin\theta - F_d\cos\theta = \frac{k}{l}u, \qquad (4)$$

where m is the total mass of the humanoid and l denotes the height of the Center of Mass (CoM). The parameters, c and k, are the damping and spring constants, respectively. The gravitational acceleration is represented as g and F_d denotes the disturbance variable. θ is the angle of the pendulum with respect to the vertical plane and u means the position input in the horizontal direction. The damping, c, and spring, k, constants are determined through system identification. To estimate the angle of the pendulum, θ, the state observer is designed based on the ZMP value measured by F/T sensors located on both ankle joints.

Forces remaining after joint compliance control are treated as disturbances, F_d, and assumed constant. Then, Eq.(4) becomes a linearized state-space representation described in Eq.(5).

$$\begin{aligned} \dot{X} &= AX + Bu \\ Y &= CX + Du. \end{aligned} \qquad (5)$$

where

$$\begin{aligned} X &= \begin{bmatrix} \theta \\ \dot{\theta} \\ F_d \end{bmatrix}, \\ A &= \begin{bmatrix} 0 & 1 & 0 \\ -\frac{k-mgl}{ml^2} & -\frac{c}{ml^2} & \frac{l}{ml^2} \\ 0 & 0 & 0 \end{bmatrix}, B = \begin{bmatrix} 0 \\ \frac{k}{ml^3} \\ 0 \end{bmatrix}, \\ C &= \begin{bmatrix} \frac{k}{mg} & \frac{c}{mg} & 0 \end{bmatrix}, D = \begin{bmatrix} -\frac{k}{mgl} \end{bmatrix}. \end{aligned}$$

According to Eq.(5), the output, Y, is equal to the location of the ZMP and the state matrix, X, is composed of the angle, θ, angular velocity, $\dot{\theta}$, of the LIPM, and disturbance, F_d, in the horizontal direction.

Now the state estimation can be found through conventional methods to design the observer shown in Eq.(6).

$$\begin{aligned} \dot{\hat{X}} &= A\hat{X} + Bu + L(Y - \hat{Y}) \\ \hat{Y} &= C\hat{X} + Du \\ \dot{\hat{X}} &= (A - LC)\hat{X} + (B - LD)u + LY, \end{aligned} \qquad (6)$$

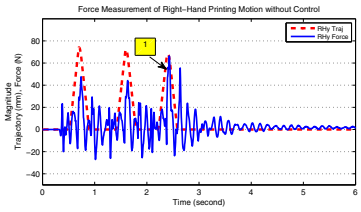

(a) **Without controls**: Right-hand trajectory and force measurement in the direction of printing (Y-direction).

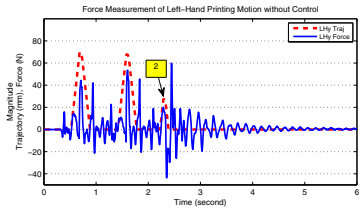

(b) **Without controls**: Left-hand trajectory and force measurement in the direction of printing (Y-direction).

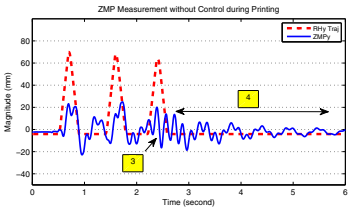

(c) **Without controls**: ZMP measurement in the direction of printing (Y-direction) and Right-hand trajectory as a reference to be compared to ZMP data.

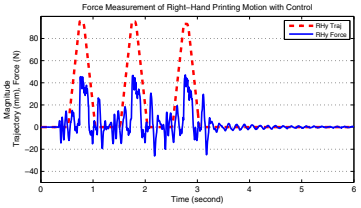

(d) **With controls**: Right-hand trajectory and force measurement in the direction of printing (Y-direction).

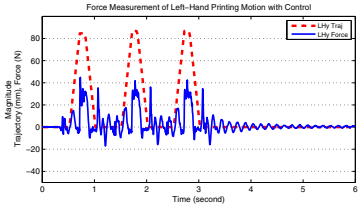

(e) **With controls**: Left-hand trajectory and force measurement in the direction of printing (Y-direction).

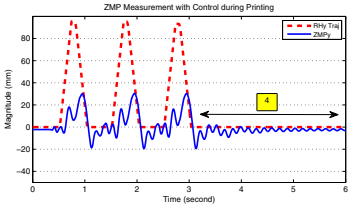

(f) **With controls**: ZMP measurement in the direction of printing (Y-direction) and Right-hand trajectory as a reference to be compared to ZMP data.

Fig. 8. Data measured from DRC-Hubo printing 3 dots on a wall; Right and left hand trajectories and force in the direction of printing.

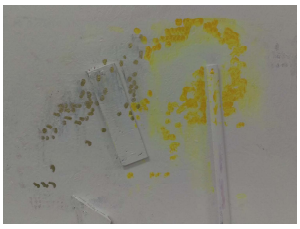

(a) Graffiti without controls

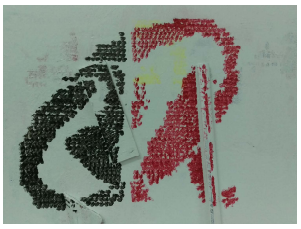

(b) Graffiti with controls.

Fig. 9. Paintings for 'RA', a logo for IEEE Robotics and Automation Society, drawn on an uneven wall by DRC-Hubo using Pointillist technique.

where $\hat{X}$ and $\hat{Y}$ are the estimated states and output, respectively. L denotes the observer gain. To reject the disturbance while being stable, the system control input, $u = -K\hat{X}$, is defined with the estimated states, $\hat{X}$, and regulator gains, K.

Fig. 6 demonstrates the performance of the controller empirically obtained from DRC-Hubo . The data in Fig. 6 is the ZMP measurements in the Y-direction (lateral) when the disturbance is applied to DRC-Hubo in the same direction. The performance of the controller (red-solid-line) is compared to the robot's natural vibration (blue-dotted-line). The following parameters are used: 77.77 kg for the total mass, 0.7752 m for the height of the CoM, 4657.9 for the spring coefficient, and 45.1950 for the damping coefficient. The regulator pole locations are empirically selected as $\begin{bmatrix}-5+i & -5-i\end{bmatrix}$ and observer pole locations are also experimentally specified as $\begin{bmatrix}-8+i & -8+i & -8\end{bmatrix}$ to estimate the states from the ZMP measurement. The controller in X-direction (forward) was implemented in the same manner.

V. EXPERIMENTAL RESULTS

A. Experimental Setup

Fig. 7(a) is DRC-Hubo (167 cm, 80 kg, 32-DOF) used for artistic work and Fig. 7(b) depicts the initial pose to do graffiti on the wall. The XYZ local frame is centered in the pelvis. The robot's feet are parallel to the wall and it's upper-body is yawed 90-degrees to face the wall. Krink markers are popular with graffiti artists and 12 mm diameter versions were used in DRC-Hubo's hands.

To verify the performance improved by the proposed control methods in this paper, DRC-Hubo prints 3-dots in the horizontal direction (X-direction). During the motion, the trajectories of the end-effectors, force exerted on wrists, and ZMP in the direction of printing (Y-direction) are measured and shown from Fig. 8(a) and Fig. 8(f). Note that for clarity, force and ZMP profiles in the figures are multiplied by -1 to flip the plots.

In this experiment, the trajectories for hands are generated with 0.2 m/s for plane motion described in Section. II-A. The acceleration, velocity limit, and hand movement constraint for printing motion in Section. III are set to $10\,\mathrm{m/s^2}$, 0.4 m/s, and 0.1 m, respectively. The force threshold for contact is defined as -20 N in the direction of printing (Y-direction). In terms of joint compliance to reduce the impact of disturbance, the proportional gains in the motor controllers for elbow, wrist yaw, and wrist pitch joints are decreased to 20.59%, 7.18%, and 12.16% of the original gain (500), respectively. There are 4 postures to draw a sub-image which contains 16 sections explained in Section. II-A. DRC-Hubo draws sections from the top to bottom by crouching. The height of the CoM locations for poses used in here are 0.9301 m, 0.7810 m, 0.6341 m, and 0.4902 m. These values are applied to the design of controller described in

Section. IV-B.

B. Data Analysis

Figs. 8(a) and (b) depict right and left trajectories and force measurements, respectively, during the motion of printing without any controls. On the other hands, Fig. 8(d) and 8(e) shows the same data but with controls developed in this paper. The number 1 highlighted in Fig. 8(a) indicates a point flicked in right-hand force profile during printing 3*rd* point. It physically means that a large impact force in a contact was acting on the body. It resulted in a significant vibration depicted in Fig. 8(c) with the number 3 highlighted, which caused missing 3*rd* dot in left hand motion arrowed by the highlighted number 2 in Fig. 8(b). This phenomena can be clearly seen in Fig. 9 explained in Section. V-C. By contrast, trajectories, force, and ZMP measurements with the same motion but where controllers were applied to show the consistent profiles with a regular pattern fluctuated. In addition, the performance of disturbance rejection is verified through a comparison of ZMP profiles indicated by the highlighted number 4 in Fig. 8(c) and 8(f).

C. Robotic Drawings - Pointillism Arts

To demonstrate the performance of DRC-Hubo drawing an image using Pointillist technique on uneven wall, a logo of IEEE Robotics and Automation Society, 'RA', was selected. The given size of the logo was 1000×600. It was converted to a 100×60 image. Except for dots in white background, the converted image contains 1016 dots. Figs. 9(a) and (b) show 'RA' on an uneven wall without and with controls, respectively. In Fig. 9(a), there are many missing dots because of vibration.

Fig. 1 shows the final result performed on September in 2015.

VI. CONCLUSION

This paper presented a biped humanoid creating graffiti style art work in human-centered environments using Pointillism. Realization of the work was composed of 3 steps; image processing, motion planning, and design of controllers. The challenges were 1) how to properly convert an artist's drawing into an image that the humanoid can represent without losing the artist's intent, 2) how to plan the motion of end-effectors printing many dots on an uneven wall without any fixed references in between the robot and ground, and 3) how to handle issues that arise from mechanical and environmental uncertainties - particularly vibrations generated by disturbances. The work in this paper mainly presented methods to overcome such challenges. Through the demonstration of the biped humanoid creating a logo design on a wall, the proposed concepts and approaches to realize an artistic work were verified.

REFERENCES

[1] G. Jean-Pierre and Z. Said, "The artist robot: A robot drawing like a human artist," in *Industrial Technology (ICIT), 2012 IEEE International Conference on*, March 2012, pp. 486–491.

[2] S. Jain, P. Gupta, V. Kumar, and K. Sharma, "A force-controlled portrait drawing robot," in *Industrial Technology (ICIT), 2015 IEEE International Conference on*, Mar 2015, Conference, pp. 3160–3165, kuka Force controlled drawing.

[3] Y. Lu, J. Lam, and Y. Yam, "Preliminary study on vision-based pen-and-ink drawing by a robotic manipulator," in *Advanced Intelligent Mechatronics, 2009. AIM 2009. IEEE/ASME International Conference on*, July 2009, Conference, pp. 578–583, important Papers. It describes many things..

[4] J. Lam, K. Lo, and Y. Yam, "Robot drawing techniques for contoured surface using an automated sketching platform," in *Automation Science and Engineering, 2007. CASE 2007. IEEE International Conference on*, Sep 2007, Conference, pp. 735–740, robot drawing to contour like egg with 3-axes machine like CNC. 1) coordinate mapping 2) trajectory generation 3) pencil manipulation. *Limited work space. Fixed.

[5] M. Srikaew, S. Cambron, R. Northrup, M. Wilkes, and K. Kawamura, "Humanoid drawing robot," in *IASTED International Conference on Robotics and Manufacturing*, 1998, Conference, very limited performance.

[6] S. Calinon, J. Epiney, and A. Billard, "A humanoid robot drawing human portraits," in *Humanoid Robots, 2005 5th IEEE-RAS International Conference on*, Dec 2005, Conference, pp. 161–166, potraits, 4DOF arm. Basically kinematic motion some force control. limited work space.

[7] S. Ali, M. Hamza Siddiqui, M. Ahmed, and S. Ahmed, "Robotic freehand drawing using visual feedback," in *Robotics, Biomimetics, and Intelligent Computational Systems (ROBIONETICS), 2013 IEEE International Conference on*, Nov 2013, pp. 232–236.

[8] H. Dang, Y. Jun, P. Oh, and P. Allen, "Planning complex physical tasks for disaster response with a humanoid robot," in *Technologies for Practical Robot Applications (TePRA), 2013 IEEE International Conference on*, Apr 2013, Conference, pp. 1–6.

[9] M. Zucker, Y. Jun, B. Killen, T. Kim, and P. Oh, "Continuous trajectory optimization for autonomous humanoid door opening," in *Technologies for Practical Robot Applications (TePRA), 2013 IEEE International Conference on*, Apr 2013, Conference, pp. 1–5.

[10] Y. Jun, J. Weisz, C. Rasmussen, P. Oh, and P. Allen, "Real-time teleop with non-prehensile manipulation," in *Technologies for Practical Robot Applications (TePRA), 2014 IEEE International Conference on*, Apr 2014, Conference, pp. *peer–review.

[11] W.-D. R. Challenge. [Online]. Available: https://en.wikipedia.org/wiki/DARPA_Robotics_Challenge

[12] N. Hogan, "Impedance control: An approach to manipulation," *American Control Conference, 1984*, pp. 304–313, 1984.

[13] O. Khatib and J. Burdick, "Motion and force control of robot manipulators," in *Robotics and Automation. Proceedings. 1986 IEEE International Conference on*, vol. 3, Apr 1986, Conference, pp. 1381–1386.

[14] L. Sentis and O. Khatib, "Synthesis of whole-body behaviors through hierarchical control of behavioral primitives," *International Journal of Humanoid Robotics*, vol. 2, no. 4, pp. 505–518, 2005.

[15] D. Wilson, "Which pwm technique is best? part 1-7," TI E2E Community Blogs, https://e2e.ti.com/blogs_/b/motordrivecontrol/archive/2012/03/19/so-which-pwm-technique-is-best-part-1.

[16] T. Park and S. Lee, "Disturbance observer based robust control for industrial robots with flexible joints," in *Control, Automation and Systems, 2007. ICCAS '07. International Conference on*, Oct 2007, Conference, pp. 584–589.

[17] S. Katsura, K. Irie, and K. Ohichi, "Wideband force control by position-acceleration integrated disturbance observer," *Industrial Electronics, IEEE Transactions on*, vol. 55, no. 4, pp. 1699–1706, April 2008.

[18] B. Cho, J. Kim, and J. Oh, "Balance strategy using the principle of energy conservation for a hopping humanoid robot," *International Journal of Humanoid Robotics*, vol. 10, p. 1350020, July 2013.

[19] J. Kim, I. Park, and J. Oh, "Walking control algorithm of biped humanoid robot on uneven and inclined floor," *Journal of intelligent and robotic systems*, vol. 48, no. 4, pp. 457–484, Apr 2007.